Car–Parrinello and path integral molecular dynamics study of the hydrogen bond in the acetic acid dimer in the gas phase

ARTICLE *in* JOURNAL OF MOLECULAR MODELING · MARCH 2011

Impact Factor: 1.74 · DOI: 10.1007/s00894-011-1020-9 · Source: PubMed

3 AUTHORS, INCLUDING:

Piotr Durlak
University of Wroclaw
14 PUBLICATIONS **72** CITATIONS

SEE PROFILE

J Mol Model (2011) 17:2995–3004
DOI 10.1007/s00894-011-1020-9

ORIGINAL PAPER

Car-Parrinello and path integral molecular dynamics study of the hydrogen bond in the acetic acid dimer in the gas phase

Piotr Durlak · Sławomir Berski · Zdzisław Latajka

Received: 1 November 2010 / Accepted: 13 February 2011 / Published online: 1 March 2011

Abstract In the paper are described studies of the double proton transfer (DPT) processes in the cyclic dimer of acetic acid in the gas phase using Car-Parrinello (CPMD) and path integral molecular dynamics (PIMD). Structures, energies and proton trajectories have been determined. The results show the double proton transfer in 450 K. In the classical dynamics (CPMD) a clear process mechanism can be identified, where asynchronized DPT arises due to coupling between the O-H stretching oscillator and several low energy intermolecular vibrational modes. The DPT mechanism is also asynchronic when quantum tunneling has been allowed in the simulation. It has been found that the calculated values of barrier height for the proton transfer depends very strongly on the used approaches. Barrier received from the free-energy profile at the CPMD level is around 4.5 kcal mol^{-1} whereas at the PIMD level is reduced to 1 kcal mol^{-1}. The nature of bonding in acetic acid dimer and rearrangement of electron density due to the proton movement has been also studied by the topological analysis of Electron Localization Function and Electron Localizability Indicator function.

Keywords Acetic acid dimer (AAD) · Double proton transfer (DPT) · Electron localisation function (ELF) · Electron localizability indicator (ELI) · Hydrogen bond · Path integrals molecular dynamics (PIMD) · Quantum effects

P. Durlak (✉) · S. Berski · Z. Latajka
Faculty of Chemistry, University of Wrocław,
14 F. Joliot-Curie Str,
50–383 Wrocław, Poland
e-mail: piotr@elrond.chem.uni.wroc.pl
URL: http://kwanty.wchuwr.pl

Abbreviations

B3LYP	Becke, Lee, Yang and Parr generalized hybrid functional
CPMD	Car-Parrinello molecular dynamics
DFT	Density functional theory
DPT	Double proton transfer
ELF	Electron Localisation Function
ELI	Electron Localizability Indicator function
MP2	Second-order Møller-Plesset perturbation method
PBE	Perdew, Burke and Ernzerhof generalized gradient functional
PCG	Preconditioned conjugate gradient method
PIMD	Path integral molecular dynamics
PI10	Ten polymer-beads model

Introduction

Proton transfer (PT) along hydrogen bonds features in some of the most fundamental oxidation/reduction processes in chemistry and biology [1, 2], with examples including the tautomeric forms of the hydrogen-bonded base pairs of DNA [3] and the many enzymes that act as proton relay systems involved in energy conversion and cell pH stabilization [4].

Recent applications of experimental and theoretical methods have made considerable progress toward understanding the mechanism of PT, and to a certain level of approximation it is now understood. From the experimental perspective direct evidence is hard to obtain, as the transfer reaction occurs on the femtosecond (10^{-15}s) timescale, requiring the use of multidimensional nonlinear coherent laser spectroscopies. There have been several recent studies on cyclic carboxylic acid dimers [5–19] and other simple

systems [10, 20], which have given rise to the discovery that the O-H stretching motions are coupled anharmonically to lower frequency vibrational modes, that are in turn responsible for modulating the length of the hydrogen bond. This basic structural mechanism establishes a continuum of potential energy surface (PES) shapes, from the double well at hydrogen bond lengths around 2.6 Å, toward a single well at around 2.4 Å. The basic structural bonding motif of the cyclic carboxylic acid dimer unit, which forms the basis of this work, can also support a double proton transfer (DPT) process, which then raises further questions concerning how the two PT steps are linked.

Several theoretical reports (based on Hartree-Fock chemical dynamics and Car-Parrinello molecular dynamics) for the cyclic formic acid dimer set out a clear DPT reaction mechanism [8, 11]. These calculations explored the classical potential energy surface (PES), where the transferring proton is required to hop, rather than tunnel, through any existing reaction barrier. The impact of quantum fluctuations on PT events through the path-integral [21–23] formalism has also been reported. Recently we extended this work to the chloroacetic acid dimer system and reported concordant results [24].

The complete mechanism for DPT under classical conditions was first proposed by Ushiyama and Takatsuka and can be summarized as follows. The first proton thermally hops to the other side of the hydrogen bond PES via a coupling of the O-H stretching and lower frequency vibrational modes without inducing large deformation of the skeleton O-C-O bonds. There then arises a small time delay while the orders of the C-O and C=O bonds on both sides of the hydrogen bond linkage switch, and the second proton is then pulled across its hydrogen bond by the increased charge on the acceptor oxygen atom. The DPT process is therefore asynchronous: the two protons do not pass the mid-points of their respective hydrogen bonds at the same time. The mechanism allowing for quantum tunneling was first put forward by Miura, which suggested a much more dynamical, almost erratic system, where the clear-cut classical mechanism steps are ignored. Crucially, PT can now occur over O–-O distances greater than 2.4 Å and there is no appreciable coupling between the O-H stretch and low frequency vibrational modes. There is also a shift to synchronous DPT behavior.

This paper is a continuation of our work on the cyclic chloroacetic acid dimer system, and we now report our results on the parent molecule under ab initio CPMD and PIMD conditions, which lend further support to the accepted mechanism for DPT under classical and quantum conditions. In addition, we report on the free energy surfaces obtained for both techniques and investigate the nature of the electronic rearrangements incurred in the DPT mechanism using a topological analysis based on the electron localization functions ELF and ELI-D.

Calculation details

Plane-wave basis set calculations

Calculations have been carried out using the CPMD program [25] version 3.13.2, with the initial molecular configuration for the acetic acid dimer optimized by the preconditioned conjugate gradient (PCG) method. The dimer was located in a simple cubic box of dimension 11.0 Å. Molecular dynamics and path integral simulations (NVT ensemble) were carried out at 450 K with a time step of 3.0 a.u. (0.072566 fs), coupled to a Nosé-Hoover chains thermostat [26] at a frequency of 3200 cm^{-1}. An electronic mass parameter of 400 a.u. was employed. Electronic exchange and correlation have been modeled using the gradient-corrected functional of Perdew, Burke and Ernzerhof (PBE) [27]. Core electrons were treated using the norm-conserving atomic pseudopotentials (PP) of Troullier and Martins [28], while valence electrons were represented in a plane-wave basis set truncated at an extended energy cut-off of 80 Ry. Two types of molecular dynamics simulation have been carried out. In the first the behavior of all atoms was treated classically (Car-Parrinello dynamics, CPMD); in the second as quantum particles (path integral dynamics, PIMD). Following the initial equilibration period, data was accrued for a further 25 ps for the Car-Parrinello dynamics on the parent model and 23 ps (imaginary-time) for the path integral dynamics simulation. The path integral simulation was carried out with ten polymer-beads (PI10) using the normal mode variable transformation. The data was visualized using the VMD program [29], with the path integral data first processed using a script by Kohlmeyer to calculate the centroid position of each set of polymer-beads [30].

Localized basis set calculations

A series of geometry optimizations, together with vibrational harmonic frequency calculations, were undertaken to localize the key stationary points on the potential energy surface (PES) of the acetic acid dimer. Calculations were performed using the Gaussian 03 package [31], utilizing the Møller-Plesset [32] correlation energy correction level truncated at the second-order (i.e., MP2), and at various DFT levels (PBE1PBE [27] and B3LYP [33, 34]), all coupled with the aug-cc-pVDZ basis set [35]. The ELF and ELI-D functions were obtained using DGrid and Basin (version 4.3) [36] on three snapshot geometries lifted directly from the CPMD trajectory which were subjected

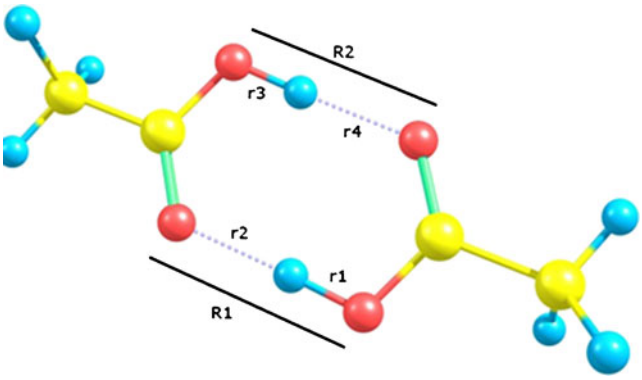

Fig. 1 Structure and atomic labeling for the acetic acid dimer

to single point energy calculations (PBE1PBE/aug-cc-pVDZ) prior to topographical analysis.

Results and discussion

A. Car-Parrinello molecular dynamics

The molecular structure of the acetic acid dimer system is shown in Fig. 1. We present in Table 1 selected optimized geometrical parameters obtained from the localized basis set calculations, along with the plane wave results (CPMD), and offer some experimental values for direct comparison. We observe that the parameters most sensitive to the choice of computational approach are the O–-O bond distances, with the localized basis sets generating results in closer agreement with the gas electron diffraction experimental results [37]. All calculations report the expected result that the O-H–-O deviates only slightly from linearity (ca. 178°); however the dynamics calculations confirmed that the structural unit is not rigid, but rather displays a large amplitude motion.

The time-evolution behavior of the bond lengths involved in the intermolecular O-H—O bond are presented in Fig. 2, from which it is evident that the dimer-system displays two different behaviors. The first is a rest phase, where each proton exhibits normal O-H vibrational behavior and remains closely associated with only one oxygen atom; the second is an active phase, where the protons quickly cross the potential energy surface and transfer to the other oxygen atoms. In total this double-proton transfer phase was observed four times over the course of the 25 ps trajectory. While these results are not particularly statistically significant, we recently reported on the chlorinated analogue, which being a stronger acid supported eight DPT events over a 35 ps trajectory. We observed a mechanism largely in agreement with that previously reported by Ushiyama et al. [11] for the formic acid dimer. As expected the acetic acid dimer reported here displays the same DPT mechanism, and for completeness we briefly report it here. First we note that the mechanism is a classical proton 'hopping' mechanism that is the proton must pass over the top of the PES barrier. This process is facilitated by a contraction in the O–-O distance from ca. 2.7 Å to around 2.3−2.4 Å, which is driven by low energy vibrational modes associated with dimer rocking and bending modes. This contraction causes a drop in the PES barrier height, thus facilitating the movement of the proton. More often than not the proton hop event follows some 10 fs later, which correlates with the O-H stretching vibration (see Fig. 3). For the acetic acid dimer our harmonic vibrational frequency calculations suggest that the corresponding low energy modes should appear at 165 and 185 cm^{-1}; 164 and 185 cm^{-1}; 157 and 180 cm^{-1}, by DFT (B3LYP; PBE1PBE) and MP2 methods, respectively. In an effort to determine whether these modes are implicated in our simulation, we have Fourier transformed the dipole autocorrelation function obtained from the dipole dynamics generated by the CPMD simulation. This approach includes all the vibrational modes and anharmonic effects. We observe common peaks in all the resulting plots at 165 and 182 cm^{-1}, confirming that the

Table 1 Calculated selected geometrical parameters after optimization compared with the average geometrical parameters from CPMD for the acetic acid dimer system (bond lengths are in Å, angles in degrees)

Parameter	B3LYP	PBE1PBE	MP2	CPMD	Expt.
	aug-cc-pVDZ	aug-cc-pVDZ	aug-cc-pVDZ	80 Ry	
R1	2.615	2.654	2.672	2.747	2.684 [37]
R2	2.615	2.654	2.672	2.752	2.684 [37]
r1	1.006	1.004	1.001	1.238	
r3	1.006	1.004	1.001	1.426	
r2	1.608	1.649	1.671	1.536	
r4	1.608	1.649	1.671	1.535	
C-O/C-O	1.314	1.324	1.334	1.336	
C=O/C=O	1.229	1.232	1.238	1.232	
∠ R1	178.2	178.9	177.6	179.2	
∠ R2	178.2	178.9	177.6	178.8	

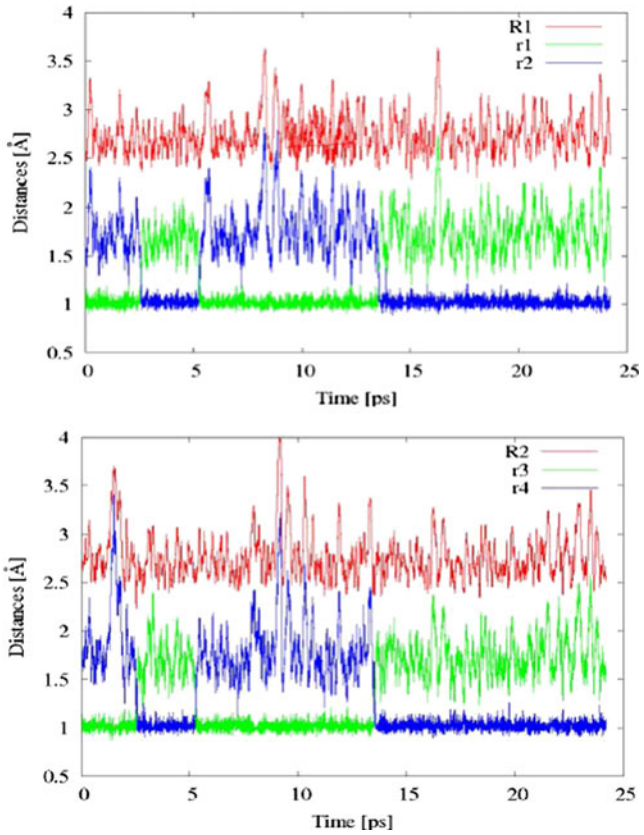

Fig. 2 Time evolutions of bonds involved in the hydrogen bonds at 450 K from the CPMD calculations

motions of the O–-O and O-H bonds are correlated at these frequencies. We now turn to consider the coupling between the two hydrogen bond linkages. As with the chloro-analogue [24] and the formic acid dimer [8–11], during the rest period the system displays asynchronous behavior (*i.e.*, as r1 increases r2 decreases, and vice versa; see Fig. 4). At the point of DPT the mechanism is a two-step process, with a re-arrangement in the skeletal O-C-O observed after the first proton has transferred (commensurate with a small time delay of less than 10 fs), in preparation for the movement of the second proton.

B. Path integral molecular dynamics

In addition to the classical dynamics, we have also studied the acetic acid dimer-system using path-integral molecular dynamics. These simulations encapsulate the effects of zero-point energy and allow the light atoms to quantum tunnel by describing each atom as a polymer-bead model. The beads interact through temperature and mass-dependent spring forces, with low temperatures and masses causing the particles to 'swell', thus mimicking the quantum motion of these nuclei.

The results are presented in Fig. 5, where the changes in hydrogen bond internal parameters (based on the arithmetic average position of the beads, *i.e.*, the centroids) immediately suggest a much more dynamical system. During this simulation the DPT phenomenon was observed about 35 times, in addition to which a small number of transient single proton transfer events, where a proton transfers from one oxygen to the other but almost immediately moves back, were also recorded. It is important to stress that it is difficult to relate the number of barrier crossings to a specific rate constant. Extensions to the PIMD method are active areas of research, with for example Geva and Voth's work on centroid dynamics [38] and Craig and Manolopoulos's work on the ring polymer MD method [39, 40] having gone some way toward the calculation of meaningful quantum reaction rate constants.

We reported on the behavior of the chloroacetic acid dimer under PIMD conditions, [22–24] as have Miura and Tuckerman for the formic acid dimer [8]. As expected, analogous results were observed for the acetic acid dimer, and we summarize them briefly for completeness. The clear

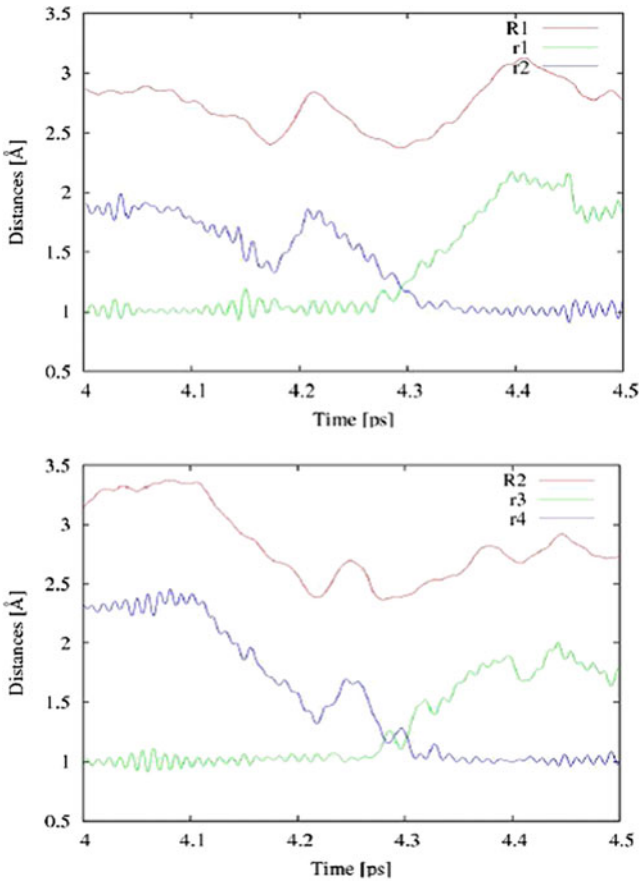

Fig. 3 Mechanism of double proton transfer (DPT) event observed in the CPMD simulation

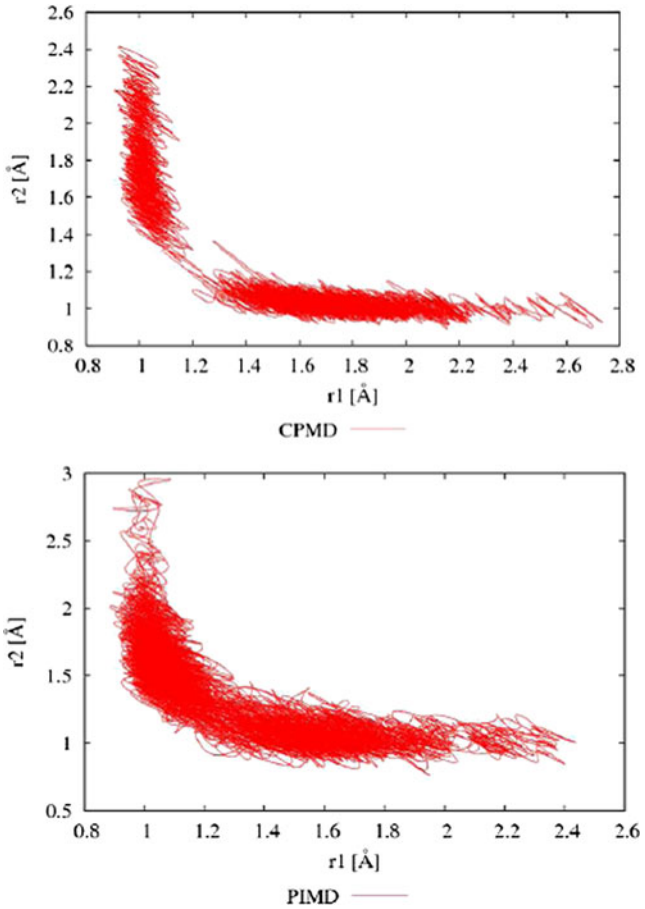

Fig. 4 Hydrogen bond distances r1 vs. r2 by (CPMD) classical dynamics and (PIMD) path integral dynamics

reaction mechanism observed for the classical surface does not hold for the quantum surface, with, *e.g.*, nearly all incidences of DFT occurring across O–-O distances which are greater than 2.4 Å, indicating a tunneling mechanism. We note also that that the average O–-O distance is considerably shorter and oscillates through a narrower range of values (2.642-2.645 Å PIMD, vs. 2.747-2.752 Å CPMD), which compares favorably with the results of a gas electron diffraction study (2.681 Å) [37]. The O-H distance in the resting phase is longer (by 0.054 and 0.016 Å) compared to the classical result (Table 1). Thus the combination of shorter O–-O and longer O-H bond lengths enhances the population of the mid-points of the two hydrogen bond distances (ca. 1.2 Å), as shown in Fig. 4. As a result, the coupling to the O-H stretching frequency is no longer a requirement, with nearly all DPT events under PIMD conditions occurring in the absence of the 10 fs delay as observed in the CPMD simulations. Finally, we note that at the actual point of proton transfer the motion of the two protons are now synchronized, which also finds agreement with the previously reported PIMD work for related systems.

C. Free-energy surfaces

Fig. 6 shows the free energy surfaces obtained from the CPMD and PIMD results, which were calculated from the equation:

$$\Delta F = -kT \ln[P(\delta)] \quad (1)$$

where k is the Boltzmann constant, T the simulation temperature, and $P(\delta)$ is the proton distribution as a function of the δ-reaction coordinate, given by δ=(rO-H – rH–-O). This parameter gives a measure of the degree of proton transfer within the hydrogen bond, with a value of zero indicating the mid-point of the hydrogen bridge.

The CPMD calculations indicate a central barrier height of around 4.5 kcal mol^{-1}. The inclusion of quantum effects drastically changes the effective potential shape, with the barrier height reduced to a value of ca. 1 kcal mol^{-1}. It is important to remember that the PIMD surface will account for some of the ZPE correction, which will be appreciable since it is the O-H stretching

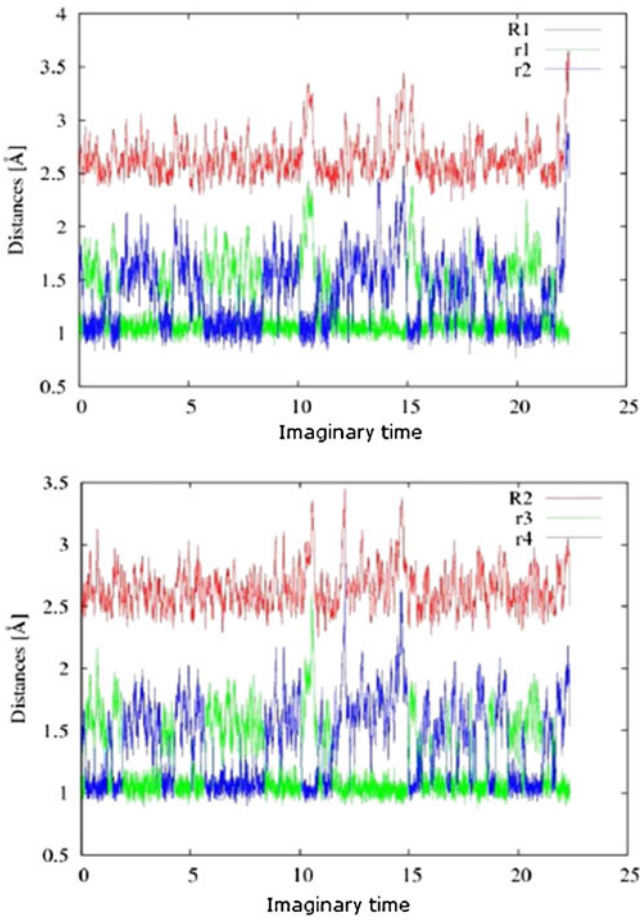

Fig. 5 Evolutions of bonds involved in the hydrogen bonds at 450 K from the PIMD calculations (based on the bead centroid position)

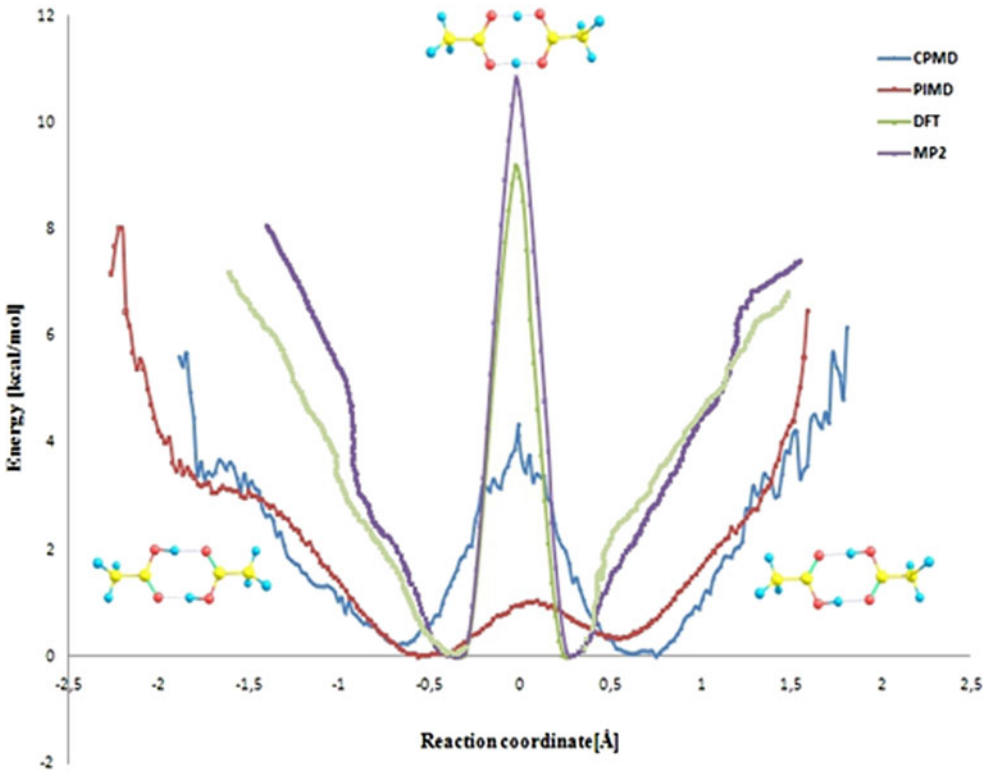

Fig. 6 Classical (blue) and quantum (red) free-energy profiles compared with the static energy barrier from DFT (green) and MP2 (violet) calculations for the double proton transfer in the acetic acid dimer

frequency that becomes imaginary at the transition point. On the other hand the energy barrier from the static calculations on the DFT and MP2 method levels indicate a central barriers height of around 9.3 kcal mol^{-1} and 10.8 kcal mol^{-1}.

Single-crystal pulsed neutron diffraction studies by Wilson et al. [41] shows that proton disorder in the benzoic acid crystal, which packs in the same carboxylic acid dimer motif, is sensitive to temperature. At 175 K the occupancy ratio for the two possible dimer configurations are 0.62/0.38, which match our gas-phase PIMD values (see Fig. 7) obtained at 450 K

D. Analysis of bonding

We now attempt to classify the nature of the hydrogen bond interaction in the acetic acid dimer system by topographical analysis of the electron localization function (ELF) [42, 43]. We focus on three structures observed in the MD trajectory: (i) the rest phase, where each proton is associated with only one well on the potential energy surface (i.e., 0 fs), (ii) when both protons are located approximately at the mid-point of their respective hydrogen-bond bridges (8 fs), and (iii) the structure observed after the first proton has transferred before the second proton begins to move (12 fs). Each structure was subjected to a localized basis set single point energy calculation at the PBE1PBE/aug-cc-pVDZ level prior to the determination of the ELF and electron localizability indicator (ELI-D) functions.

Before the proton transfer event (0 fs) the topographical analysis indicates that the two molecules are separated by a region with low ELF-values (Fig. 8a), which are associated with small values of low electron density. Electrons in the H1–-O2 and H1'—O2 regions have a small degree of localization. When both protons are close to the mid-points

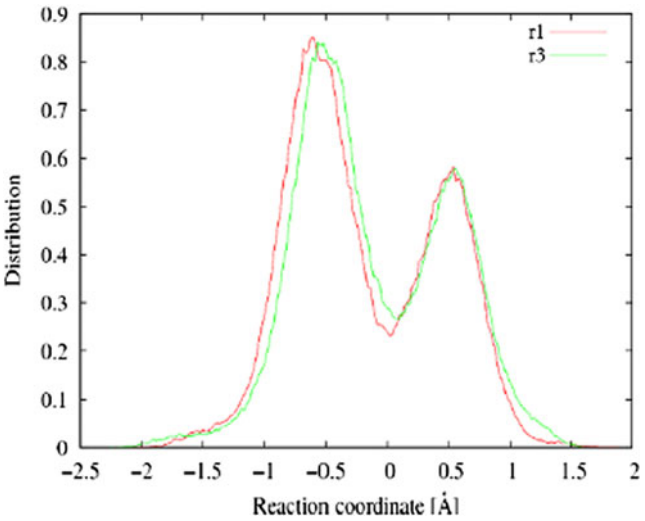

Fig. 7 Distribution function of the protons from the PIMD simulation

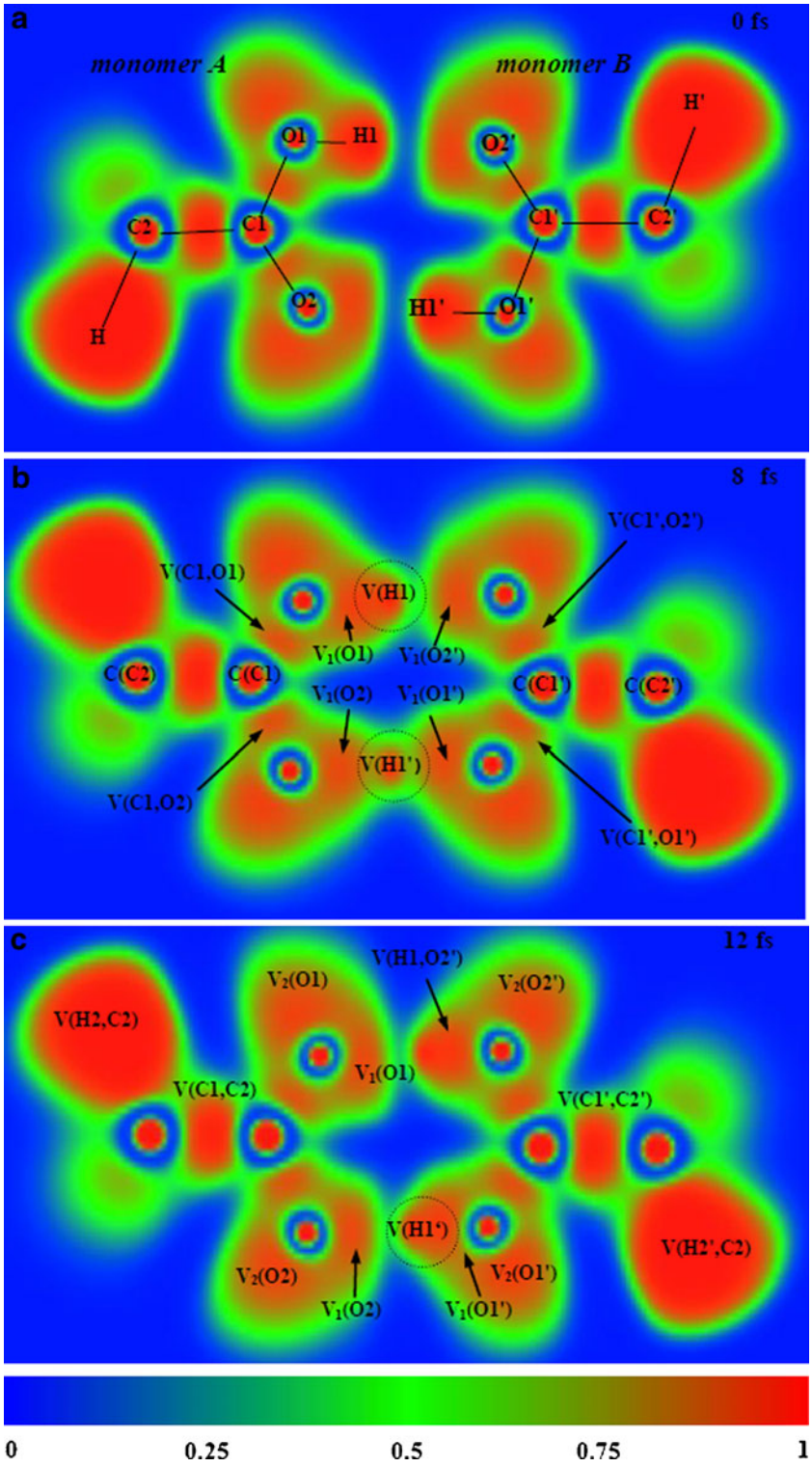

Fig. 8 2D plot of the ELF function in the molecular plane of the acetic acid dimer. Values of the basin populations have been calculated for the ELI-D function

of their hydrogen bonds (Fig. 8b) protonated basins of the monosynaptic type V(H1), V(H'), corresponding to 'dressed' protons, are observed. There exists some asymmetry, however, which is clearly visible on the ELF plot. The basin around H1 in the lower hydrogen bond bridge indicates that this proton is separated by an area of low ELF value from the lone pairs of both O1' and O2, while the basin around the other proton clearly shows a separation from O2' only. In Fig. 8c the proton in the upper hydrogen bond bridge has transferred but the movement of the proton in the lower bridge is restrained around its original position at 0 fs. We therefore have an ionic system and once again

Table 2 The basin populations (*N*) in the acetic acid dimer

Basin/N[e]	0 [fs]	8 [fs]	12 [fs]
Monomer A			
C(C1)	2.10	2.10	2.10
C(C2)	2.10	2.10	2.10
C(O1)	2.14	2.14	2.14
C(O2)	2.14	2.14	2.14
V_1(O1)	-	2.07	2.30
V_2(O1)	4.12	3.66	3.16
V_1(O2)	2.52	1.88	2.19
V_2(O2)	2.88	3.46	3.61
V(C1,C2)	2.11	2.11	2.11
V(C1,O1)	1.76	1.88	2.17
V(C1,O2)	2.28	2.21	1.83
V(H1,O1)	1.91	-	-
V(H,C2)	1.97	1.97	1.97
V(H1,C2)	1.97	1.97	1.97
V(H3,C2)	2.00	2.00	2.00
V(H1)	-	0.40	-
V(H1')	-	0.40	0.32
Monomer B			
C(C1')	2.10	2.10	2.10
C(C2')	2.10	2.10	2.10
C(O1')	2.14	2.14	2.14
C(O2')	2.14	2.14	2.14
V_1(O1')	-	1.70	1.93
V_2(O1')	4.12	3.94	3.35
V_1(O2')	2.52	1.69	-
V_2(O2')	2.88	3.53	3.86
V(C1',C2')	2.11	2.12	2.13
V(C1',O1')	1.76	1.89	2.24
V(C1',O2')	2.28	2.23	1.84
V(H1',O1')	1.91	-	-
V(H1,O2')	-	-	2.14
V(H',C2')	1.97	1.97	1.96
V(H1',C2')	1.96	1.97	1.97
V(H3',C2')	2.00	2.00	2.00

we observe that the two molecular domains are separated by low electron density and ELF values.

The observations on the ELF plots can be quantified at a deeper level by using ELI-D function, which depicts the average number of electrons per fixed fraction of a same-spin electron pair in a compact region (so-called micro-cell) in space. The value for the ELI-D ($\Upsilon_D{}^{\sigma}$) at position a_i where such micro-cell is centered is defined as:

$$\Upsilon_D^{\sigma}(a_i) \approx \rho(a_i)\frac{V_i}{(D^{\sigma\sigma})^{\frac{3}{8}}} = \rho(a_i)\widetilde{V}_D(a_i) \qquad (2)$$

and $\rho(a_i)$ is the electron density at position a_i, V_i volume of micro-cell, $D^{\sigma\sigma}$ the number of same-spin electron pairs and V_D (a_i) pair-volume distribution [44].

The topological analysis reveals the basins associated with the attractors of the ELI-D field, *i.e.*, the (3,-3) critical points, and an integration of the electron density over these basins provides the basin populations (N) (see Fig. 8). It is worth mentioning that at the DFT level the ELF and ELI-D functions yield the same results. At 0 fs the two H1-O1, H1'-O1' covalent bonds are characterized by the disynaptic basins V(H1,O1), V(H1',O1') to which 1.91e are assigned (see Table 2), and thus according to the Lewis structure they may be characterized as single-type bonds. As expected a most interesting bonding situation appears in the 8 fs snapshot image, where both protons are ascribed to monosynaptic non-bonding basins V(H1), V(H1') containing 0.39 and 0.40e, respectively. It is obvious from this that the proton "trails" some amount of the electron density and the description as a "dressed" proton is fully justified. At 12 fs, after the single proton transfer event, the H1-O2' bond is already established and the population of the bonding disynaptic basin V(H1,O2') equals 2.14e, which is within the range expected for a formal single O-H bond. For the other proton, which is yet to transfer, a localized monosynaptic basin comprising 0.32 e is observed. The electron density of the H1'-O2 bond resides temporarily in the V_2(O2) basin, to which the relatively large basin population of 3.61e is ascribed.

From the data presented in Table 2 we conclude that very large electron rearrangements are observed in the two subunits of the acetic acid dimer due to protons movements in hydrogen bridges, with the bulk of the charge movement occurring within the carboxylic acid groups. The 0 fs image clearly displays a C-O single (1.320 Å, basin population 1.76e) and double (1.225 Å, basin population 2.28e) bond. At 12 fs the positions of the heavy atoms do not change and yet the electron occupancies vary substantially (2.17e and 1.83e for the single and double bonds, respectively). Thus we observe that the electronic rearrangement precedes the structural rearrangement, which of course is in accordance with the Frank-Condon principle. These results therefore fully support the mechanism for DPT first put forward by Ushiyama, namely following the transfer of the first proton (which is 'pushed' across the potential energy surface by the O-H stretching motion coupling to low energy dimer rocking and bending motions), which occurs without any substantial deformation of the heavy atom framework, the second proton is then 'pulled' across by an attraction to the build up of charge resulting on the acceptor oxygen atom following O=C-O/O-C=O rearrangement.

Finally, we comment on the degree of charge transfer observed in the three snapshot images, as provided from the ELI-D analysis. For the geometry at 0 fs the charge transfer

between the two acetic acid monomers is below the numerical accuracy of the computational method (< 0.02e). At 8 fs each proton carries a positive charge of around 0.6e, while the two heavy atom fragments carry charges of −0.52 and −0.68e, a rather substantial difference for a small degree of asymmetry. At 12 fs one of the CH_3COOH molecules is formed with new bond H1-O2' and it carries small positive charge δ=+0.10e. The "dressed" proton which is not yet transferred has slightly more positive charge (δ= +0.68e) than at 8 fs and the $[CH_3COO]^{\delta-}$ anion, carries negative charge of −0.79e.

Conclusions

We have studied the classical and quantum reaction pathways for the DPT event in the cyclic acetic acid dimer system, and found a mechanism that supports that previously reported for the formic acid and dichloroacetic acid dimer systems.

Modeling the quantum behavior of the atoms by 10-bead polymer model dramatically altered the reaction pathway and increased the number of DPT events. The criteria observed for DPT under classical (CPMD) conditions are seemingly relaxed, with the two protons transferring in a synchronous fashion over donor-acceptor distances which are typically greater than 2.4 Å, and without the delay attributed to the approach frequency n O-H. At the actual point of DPT, the heavy skeletal O-C-O and hydrogen atoms all move simultaneously. There are also significant changes in the heavy atom geometry, leading to shorter and more centered hydrogen bond linkages. The average O–-O distance at the CPMD level is 2.75 Å and in very good accord with available experimental data from the gas phase experiment (2.68 Å) [37]. Thus we note that the introduction of a path integral treatment, at even the modest levels reported here, can significantly improve upon the thermally average structure.

From the CPMD calculations it was shown that the O-H-–O bridge is not rigid, with the O–-O distance being described by a large amplitude motion. If the distance between two heavy atoms of the H-bond is short enough, as observed for the acetic acid dimer, the barrier for proton motion is small enough that thermal hop of the proton over the barrier is possible. The CPMD calculations indicate a central barrier height of around 4.5 kcal mol^{-1}. The inclusion of quantum effects drastically changes the effective potential shape, with the barrier height reduced to a value of ca. 1 kcal mol^{-1}. It is important to remember that the PIMD surface will account for some of the ZPE correction, which will be appreciable since it is the O-H stretching frequency that becomes imaginary at the transition point. On the other hand the energy barrier from the static calculations on the DFT and MP2 method levels indicate a central barriers height of around 9.3 kcal mol^{-1} and 10.8 kcal mol^{-1}.

It is also important to note that standard ab initio calculations only gives the value of the barrier height along the proton's reaction path; it cannot be considered the absolute criterion for the possibility of proton motion.

Acknowledgments The authors would like to gratefully acknowledge the Ministry of Science and Higher Education of Poland for the support of this research; Grant No. NN 204 0958 33. Thanks also are due to the Academic Computer Centre in Gdansk (CI TASK) for the use of the Galera-ACTION Cluster and the Wroclaw Centre for Networking and Supercomputing (WCSS) for the use of the Nova Cluster.

References

1. Müller A, Ratajczak H, Junge W, Diemann E (1992) Electron and Proton Transfer in Chemistry and Biology. Elsevier, Amsterdam
2. Limbach HH, Manz J (1998) Hydrogen transfer: experiment and theory. Ber Bunsenges Phys Chem 102:289–586
3. Bertran J, Oliva A, Rodrigues-Sabtiago L, Sodupe M (1998) Single versus double proton-transfer reactions in Watson-Crick base pair radical cations. Theor Study J Am Chem Soc 120:8159–8167
4. Williams RJP (1988) Proton Circuits in Biological Energy Interconversions. Annu Rev Biophys Biophys Chem 17:71–97
5. Chang YT, Yamaguchi Y, Miller WH, Schaefer-III HFJ (1987) An analysis of the infrared and Raman spectra of the formic acid dimer (HCOOH)2. J Am Chem Soc 109:7245–7253
6. Shida N, Barbara PF, Almlöf J (1991) A reaction surface Hamiltonian treatment of the double proton transfer of formic acid dimer. J Chem Phys 94:3633–3643
7. Kim YJ (1996) Direct dynamics calculation for the double proton transfer in formic acid dimer. J Am Chem Soc 118:1522–1528
8. Miura S, Tuckerman ME, Klein ML (1998) An *ab initio* path integral molecular dynamics study of double proton transfer in the formic acid dimer. J Chem Phys 109:5290–5299
9. Loerting T, Liedl KR (1998) Toward elimination of discrepancies between theory and experiment: Double proton transfer in dimers of carboxylic acids. J Am Chem Soc 120:12595–12600
10. Fernando-Ramos A, Smedarchina Z, Rodriges-Otero J (2001) Double proton transfer in the complex of acetic acid with methanol: Theory versus experiment. J Chem Phys 114:1567–1574
11. Ushiyama H, Takatsuka K (2001) Successive mechanism of double-proton transfer in formic acid dimer: A classical study. J Chem Phys 115:5903–5912
12. Hayashi S, Umemura J, Kato S, Morokuma K (1984) *Ab initio* molecular orbital study on the formic acid dimer. J Phys Chem 88:1330–1334
13. Madeja F, Havenith M (2002) High resolution spectroscopy of carboxylic acid in the gas phase: Observation of proton transfer in (DCOOH)2. J Chem Phys 117:7162–7168
14. Remmers K, Meerts WL, Ozier I (2000) Proton tunneling in the benzoic acid dimer studied by high resolution ultraviolet spectroscopy. J Chem Phys 112:10890–10894
15. Antoniou D, Schwartz SD (1998) Proton transfer in benzoic acid crystals: Another look using quantum operator theory. J Chem Phys 109:2287–2293

16. Car R, Parrinello M (1985) Unified Approach for Molecular Dynamics and Density-Functional Theory. Phys Rev Lett 55:2471–2474
17. Dreyer J (2005) Density functional theory simulations of two-dimensional infrared spectra for hydrogen-bonded acetic acid dimers. Int J Quantum Chem 104:782–793
18. Heyne K, Huse N, Dreyer J, Nibbering ETJ, Elsaesser T, Mukamel S (2004) Coherent low-frequency motions of hydrogen bonded acetic acid dimers in the liquid phase. J Chem Phys 121:902–913
19. Heyne K, Huse N, Nibbering ETJ, Elsaesser T (2003) Ultrafast coherent nuclear motions of hydrogen bonded carboxylic acid dimers. Chem Phys Lett 369:591–596
20. Stenger J, Madsen D, Dreyer J, Nibbering ETJ, Hamm P, Elsaesser T (2001) Coherent response of hydrogen bonds in liquids probed by ultrafast vibrational spectroscopy. J Phys Chem A 105:2929–2932
21. Tuckerman ME, Marx D, Klein ML, Parrinello M (1996) Efficient and general algorithms for path integral Car-Parrinello molecular Dynamics. J Chem Phys 104:5579–5588
22. Tuckerman ME, Berne BJ, Martyna GJ, Klein ML (1993) Efficient molecular dynamics and hybrid Monte Carlo algorithms for path integrals. J Chem Phys 99:2796–2805
23. Marx D, Parrinello M (1994) Ab initio path-integral molecular dynamics. Z Phys B Condens Matter 95:143–144
24. Durlak P, Morrison CA, Middlemiss DS, Latajka Z (2007) Car-Parrinello and path integral molecular dynamics study of the hydrogen bond in the chloroacetic acid dimer system. J Chem Phys 127:064304–064311
25. CPMD, http://www.cpmd.org, Copyright IBM Corp 1990–2008, Copyright MPI für Festkörperforschung Stuttgart 1997–2001
26. Martyna J, Klein ML, Tuckerman M (1992) Nosé-Hoover chains: The canonical ensemble via continuous dynamics. J Chem Phys 97:2635–2643
27. Perdew JP, Burke S, Ernzerhof M (1996) Generalized gradient approximation made simple. Phys Rev Lett 77:3865–3868
28. Troullier N, Martins JL (1991) Efficient pseudopotentials for plane-wave calculations. Phys Rev B 43:1993–2006
29. Humphrey W, Dalke A, Schulten K (1996) VMD: Visual molecular dynamics. J Mol Graph 14:33–38
30. Kohlmeyer A, Forbert H (2004) traj2xyz.pl-ver.1.4
31. Frisch MJ et al. (2004) Gaussian03, Revision C.02. Gaussian Inc, Wallingford
32. Møller C, Plesset MS (1934) Note on an Approximation Treatment for Many-Electron Systems. Phys Rev 46:618–622
33. Lee C, Yang W, Parr RG (1988) Development of the Colle-Salvetti correlation-energy formula into a functional of the electron density. Phys Rev B 37:785–789
34. Becke AD (1988) Density-functional exchange-energy approximation with correct asymptotic behavior. Phys Rev A 38:3098–3100
35. Kendall RA, Dunning TH, Harrison RJ (1992) Electron affinities of the first–row atoms revisited. Systematic basis sets and wave functions. J Chem Phys 96:6796–6806
36. Kohout M (2004) Basin version 4.3, DGrid version 4.3
37. Derissen JL (1871) A reinvestigation of the molecular structure of acetic acid monomer and dimer by gas electron diffraction. J Mol Struct 7:67–80
38. Geva E, Shi Q, Voth GA (2001) Quantum-mechanical reaction rate constants from centroid molecular dynamics simulations. J Chem Phys 115:9209–9222
39. Craig IR, Manolopoulos DE (2005) Chemical reaction rates from ring polymer molecular Dynamics. J Chem Phys 122:084106–084117
40. Craig IR, Manolopoulos DE (2005) A refined ring polymer molecular dynamics theory of chemical reaction rates. J Chem Phys 123:034102–034111
41. Wilson CC, Shankland N, Florence AJ (1996) Direct determination of the temperature dependence of proton transfer in the benzoic acid dimer by single crystal neutron diffraction. Chem Phys Lett 253:103–107
42. Becke AD, Edgecombe KE (1990) A simple measure of electron localization in atomic and molecular systems. J Chem Phys 92:5397–5403
43. Silvi B, Savin A (1994) Classification of chemical bonds based on topological analysis of electron localization functions. Nature 371:683–686
44. Kohout M (2004) A measure of electron localizability. Int J Quantum Chem 97:651–658